 doi:10.20944/preprints201703.0185.v1

Article

Design, Fabrication and Analysis of Threshold-Value Judging Mechanism in MEMS Safety and Arming Device

Dakui Wang [1], Wenzhong Lou [1], Yue Feng [1,*] and Fufu Wang [2]

[1] National Key Laboratory of Electro-Mechanics Engineering and Control, School of Mechanical-electronic Engineering, Beijing Institute of technology, Beijing 100081, China; wangdakui1987@163.com (D.-K.W.); louwz@bit.edu.cn (W.-Z.L.); fengyue@bit.edu.cn (Y. F.)

[2] Technology and Engineering Center for Space Utilization, Chinese Academy of Sciences, Beijing 100081, China; wangfufu2004@sina.com

* Correspondence: fengyue@bit.edu.cn; Tel.: +86-18310169212

Abstract: In order to meet the military requirements of the fuze, such as precision strike, efficient mutilates ability and low collateral damages, the microminiaturization is an inevitable trend of secure system. Based on the silicon-based MEMS S&A device designed by our term, the design principles of each module and fabrication process are introduced. The average fracture strength and Young's modulus of the silicon are 726MPa and 175GPa from the tensile test, respectively. From Hopkinson impact experiment, we can get the threshold-value judging mechanism being safety under the impact overload of 20526g, and this value is much more than the standard of the drop overload 12000g; the arming value under the centrifugal overload obtained from theory, simulation and experiment is at the range of 28200g and 32000g, it shows that the threshold-value judging mechanism can be arming compared with the value 35951g of design principle. Therefore, the threshold-value judging mechanism can meet the design requirements of overload. Furthermore, the relationship of fracture threshold-values obtained by different theories is found out through parametric design method, as shown in Figure 14, it provides the theory evidence to the follow parametric design.

Keywords: MEMS S&A device; threshold-value judging mechanism; fabrication process; tensile test; theoretical, simulation and experimental analysis; parametric design method

1. Introduction

MEMS is a relatively new and fast-growing field in microelectronics [1-3]. MEMS is commonly used as actuators, sensors, and radio frequency and micro fluidic components, as well as bio-composites, with a wide variety of applications in health care, automotive, and military industries. It is expected that the market for MEMS will grow to over $30B by 2050 [4-7].

Weapons are mainly mechanical equipment based on the mechanical processing technology in twentieth century, and are quickly into the intelligent, information and miniaturization in twenty-first century [8-10]. The application of MEMS technology is inevitable trend of the development of modern weapons and equipment. With the application of weapon is more widely, fuze as a function module of the weapon, and the function of fuze is more than ever [11]. In order to place more modules in the fuze, it is needed to apply the MEMS technology on the Safety and Arming device, which is the key mechanism about ensuring the safety in handling transportation and storage, meanwhile, it is the reliable arming with the launch overload in fuze [19-21].

 doi:10.20944/preprints201703.0185.v1

MEMS S&A device have obvious advantages compared to the traditional S&A device, such as small size, light weight and low cost [15-18]. The MEMS S&A device can make more space, place more functional modules and decrease the charge, and then improve the accuracy of ammunition, combat power and cost-effectiveness ratio.

At present, there are two routes of the miniaturization for the MEMS S&A device [19-21]. One of routes is non-silicon-based route and the other one is silicon-based route. Non-silicon-based route is mainly based on nickel and copper materials with the LIGA or UV-LIAG process, one of the advantages is that it is widely chosen material and can obtain the structure with higher depth and width. One of the disadvantages is that it cannot be integrated processing, and needs micro-assembly tasks. Silicon-based route is mainly based on silicon material with the DRIE or SOI process, the advantages are the process has a good compatibility with the traditional microelectronics process, which can achieve integration of processing and realize the miniaturization. Its disadvantages are that the impact of silicon material is relatively poor [22-24].

Silicon-based route is the development direction of the future MEMS S&A device [25-28]. The process of the Silicon-based route can be integrated with microelectronics, and make the S&A device become an independent chip module, and other modules are integrated together to achieve the conception of 'fuze on chip' [29-31]. Aiming at the conception of 'fuze on chip', our term puts forward a silicon-based MEMS S&A device innovatively. At the same time, the mechanical environment sensing layer is fabricated periodically [32-34]. Furthermore, the various modules of the mechanical environment sensing layer should be experimented and simulated.

A few works have been carried out for detailed analysis of the mechanical environment sensing layer in MEMS S&A device. This paper aims to verify the feasibility of the designed threshold-value judging mechanism in MEMS S&A device. First, the simplified threshold-value judging mechanism is fabricated and the mechanical properties of silicon materials are tested. Next, the safety of the threshold-value judging mechanism under the drop overload of service processing is confirmed through the Hopkinson impact experiment. Then, the theoretical and simulation models of the threshold-value judging mechanism are established, which the influence of the centrifugal force and the parameters for the threshold-value connection units are parametric studied based on the established models. Finally, the experimental results are presented, and the corresponding theoretical and simulation models are verified quantitatively. The research can provide fundamental knowledge for optimizing model parameters.

2. Design and fabrication

2.1. Design principles

The monolithic structure of silicon-based MEMS S&A device, which our term designed, is shown in Figure 1. The overall size of the silicon-based MEMS S&A device is 11mm×10mm×0.5mm. The MEMS S&A device is mainly used for rotating ammunition, and it is mainly divided into two parts, one is the circuit control layer and the other is mechanical environment sensing layer. The overall size of the circuit control layer is 11mm×10mm×0.1mm, and its function is to realize remote arming and detonate booster explosive. The circuit control layer is mainly composed of a frame, an electrothermal actuator component, a moving slider which is bonded to the main centrifugal slider of the mechanical environment sensing layer at the bottom and a silicon semiconductor bridge is used for detonating booster explosive. The overall size of the mechanical environment sensing layer is 11mm×10mm×0.4mm, it is mainly composed of a frame, a inertial safety device, a sub-centrifugal slider, a main centrifugal slider, an impact release mechanism, a threshold-value judging mechanism and a locking mechanism, as shown in Figure 1.

The design principles of silicon-based MEMS S&A device are as follows. The inertial safety device and other mechanisms of the mechanical environment sensing layer cannot achieve arming under the condition of extreme drop overload in service processing; under the condition of launch overload (recoil overload and centrifugal force), the inertial safety device, the threshold-value judging mechanism and the impact release mechanism can realize arming in this order. The arming

Preprints (www.preprints.org) | NOT PEER-REVIEWED | Posted: 24 March 2017 doi:10.20944/preprints201703.0185.v1

process of the mechanical environment sensing layer is as follows. Firstly, the slider of the inertial safety device under the recoil overload overcomes the elasticity of the recoil MEMS spring, next slides to the bottom and is locked at the bottom by the recoil locking mechanism. Then, under the centrifugal force, the connection nodes of the threshold-value judging mechanism fracture, the sub-centrifugal slider move in the direction of the centrifugal force and impact the connection nodes of the impact release mechanism, thus release the main centrifugal slider, At the same time, the sub-centrifugal slider is limited to a predetermined position by a locking mechanism; the main centrifugal slider continues to move in the direction of the centrifugal force under the centrifugal force, finally, it is limited to a predetermined position by a locking mechanism. At this time, the detonation transmission hole is aligned with the electric detonator and the booster pellet, the MEMS S&A device is in readiness. In addition, the barycenter position of the main centrifugal slider and the sub-centrifugal slider, as well as the position of rotation axis for the projectile is shown in Figure 2. The maximum recoil overload, the launching overload pulse width and the maximum rotating speed corresponding to different caliber ammunitions, as described in Table 1. In this study, using 35mm caliber ammunition as design criteria, then the overload curve of service processing and launch overload curve, as Figure 2 is shown.

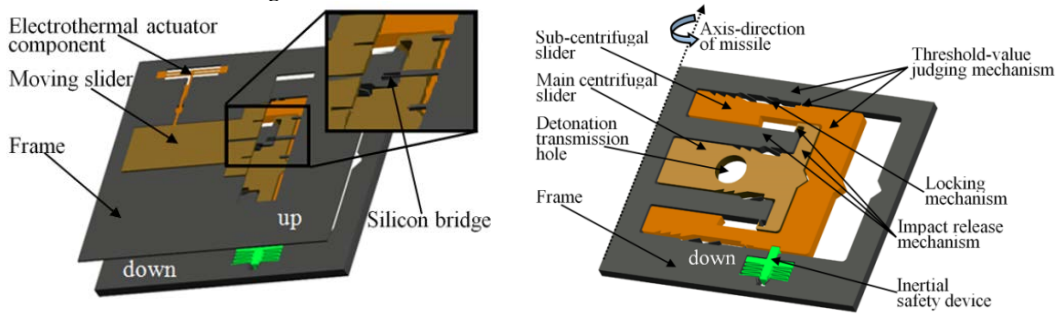

(**a**) (**b**)

Figure 1. (**a**) The designed MEMS S&A device; (**b**) Mechanical environment sensing layer

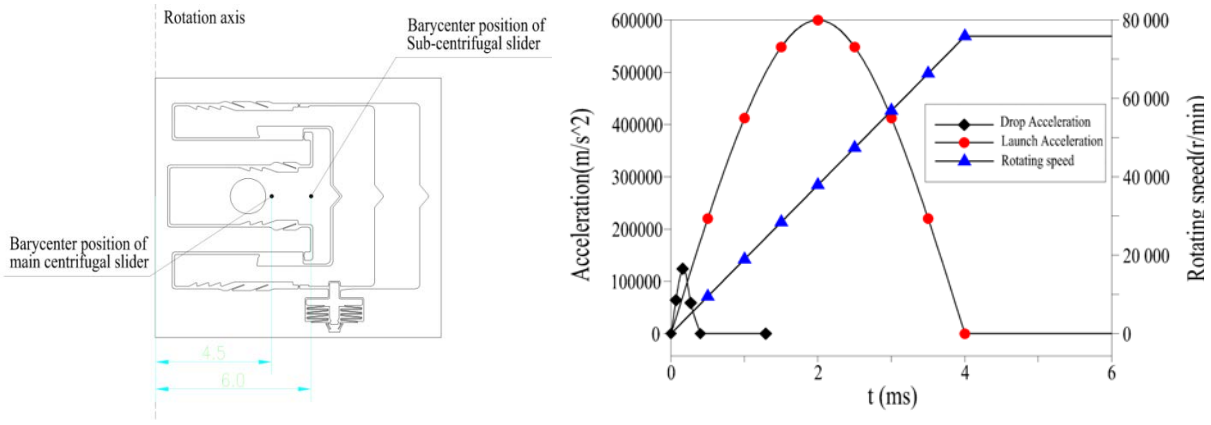

(**a**) (**b**)

Figure 2. (**a**) Barycenter position of the main centrifugal slider and the sub-centrifugal slider, as well as the position of rotation axis for the projectile; (**b**) The overload curve of service processing and luanch overload curve

Table 1. The launch environment of different caliber ammunitions.

Ammunition caliber (mm)	Maximum recoil overload (g)	Launch overload pulse width (ms)	Maximum rotating speed (r/min)
25	59734	4	82286
35	59500	4	73918
130	20000	13	10000
155	18000	15	6000

Preprints (www.preprints.org) | NOT PEER-REVIEWED | Posted: 24 March 2017 doi:10.20944/preprints201703.0185.v1

2.2. Fabrication process

At present, the mechanical environment sensing layer has been fabricated by bulk silicon processing and bonding technologies. It is mainly composed of a silicon-based mechanical environment sensing layer and the BCB bonded glasses on the upper and the lower sides. Figure 3. shows the micro fabrication process of the mechanical environment sensing layer. The detailed processing technique of the mechanical environment sensing layer is as follows.

（a）Wafer preparation. Using silicon wafer as the substrate, the resistivity of the silicon wafer is 2~4Ω.cm, and the size is 4 inches;

（b）Physical vapor deposition (PVD). Sputtered aluminum layer on the back ;

（c）Physical vapor deposition (PVD). Sputtered aluminum layer on the front ;

（d）Structural lithography. Graphical fabrication of the structure ;

（e）Aluminum corrosion. Graphical fabrication of the front aluminum layer, and the composite mask is formed with the photoresist ;

（f）Deep reactive ion etching (DRIE). Graphical fabrication of the silicon wafer (see the Figure 4.) ;

（g）Photoresist removal. Thoroughly clean the surface of silicon wafer by using concentrated sulfuric acid and hydrogen peroxide ;

（h）Wafer preparation. Using glass wafer as the substrate ;

（i）BCB lithography. Graphical fabrication of BCB ;

（j）BCB bonding. The graphical BCB is bonded to the back of the graphical silicon wafer;

（k）Wafer preparation. Using glass wafer as the substrate ;

（l）BCB lithography. Graphical fabrication of BCB ;

（m）BCB bonding. The graphical BCB is bonded to the front of the graphical silicon wafer, then the three-layer structure of glass-silicon-glass is formed ;

（n）Wafer dicing. The whole three-layer structure is divided into multiple independent units.

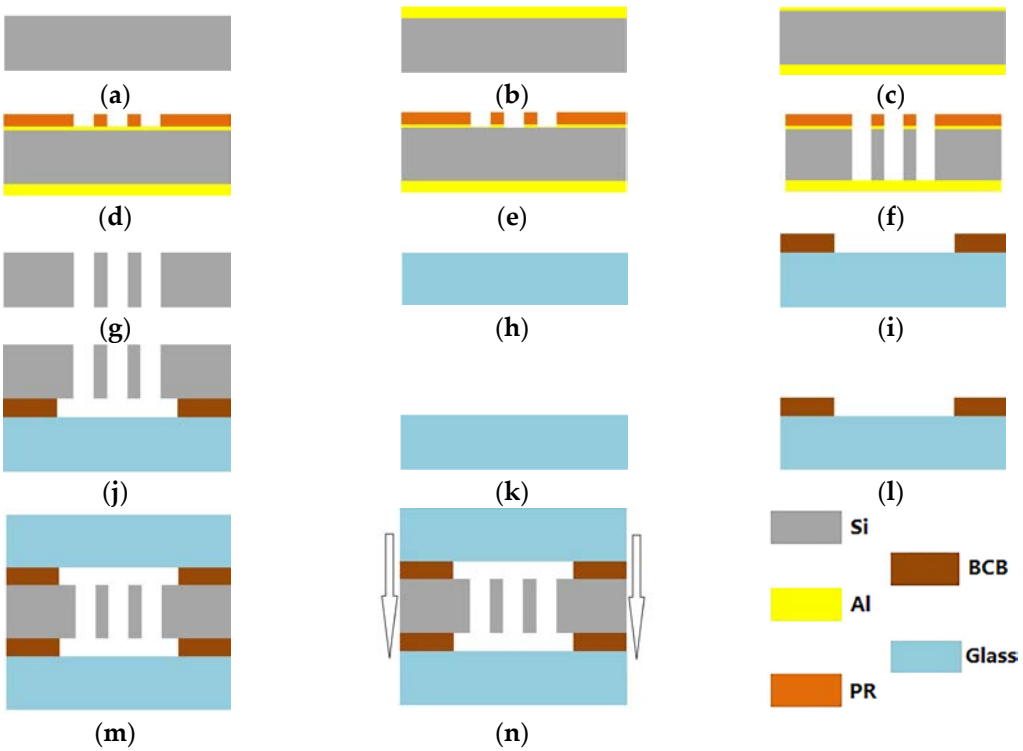

Figure 3. Fabrication process of the mechanical environment sensing layer. (**a**) Wafer preparation; (**b**) PVD Al 2um; (**c**) PVD Al 2000A;(**d**) Structural lithography;(**e**) Aluminum corrosion; (**f**) DRIE; (**g**) Photoresist removal; (**h**) Wafer preparation; (**i**) BCB lithography; (**j**) BCB bonding; (**k**) Wafer preparation; (**l**) BCB lithography; (**m**) BCB bonding;(**n**) Wafer dicing.

Preprints (www.preprints.org) | NOT PEER-REVIEWED | Posted: 24 March 2017 doi:10.20944/preprints201703.0185.v1

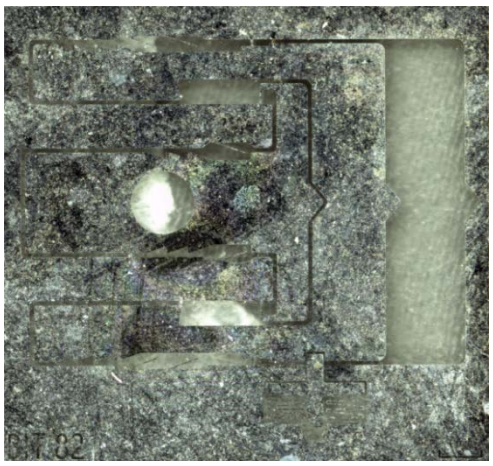

Figure 4. Structure of the mechanical environment sensing layer before BCB bonding

3. Tests of mechanical properties for silicon materials

The tensile test of the micro sample can be carried out by the micro force tensile testing machine (see Figure 5.), and then we can get the mechanical properties of silicon materials. The device is a horizontal tensile testing machine, it can be used to carry out micro force tensile test for various materials and devices, and the equipment is mainly composed of horizontal frame, force sensor, displacement sensor, air supply component, computer control system, fixed stage and so on.

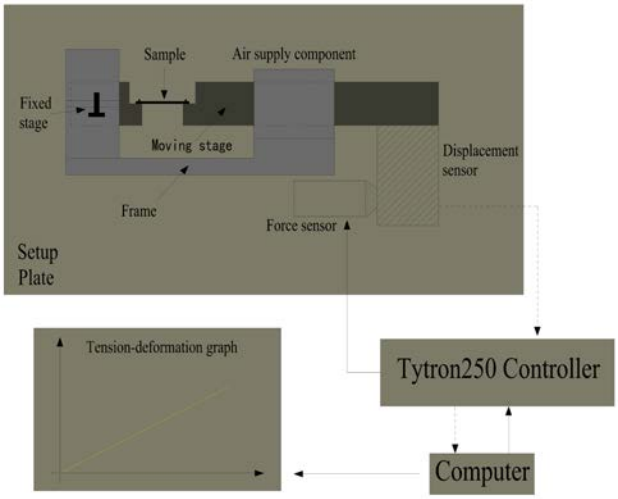

Figure 5. Schematic view of the testing equipment

The micro sample is mounted on the two mechanical fixtures of the loading unit. When the computer sends the commands which is a specific waveform signal to the controller, the signal can be transmitted to the moving end of the loading unit, and drive the moving end of the loading unit to move, then mechanical test of micro specimen is carried out. In this study, the micro samples are taken from the same batch of silicon wafers used in fabrication process. The cross sections of the tested micro sample are 0.3×0.1mm, 0.4×0.1mm, 0.5×0.1mm and 0.6×0.1mm, respectively; the lengths of the tested micro sample are 1.5mm and 2.4mm, respectively. The cross sections and the lengths of the micro sample are freely combined, and 8 groups of tests are carried out. One of the stress-strain curves of the micro sample during micro force tensile test is shown in Figure 6. Therefore, according to the stress-strain curves of the micro sample, we can get the young's modulus and fracture strength of the silicon. Computing the average of the 8 groups of test results, we can get the average young's modulus of the silicon material is E=175GPa, and average fracture strength is σ_s =726Mpa.

Preprints (www.preprints.org) | NOT PEER-REVIEWED | Posted: 24 March 2017 doi:10.20944/preprints201703.0185.v1

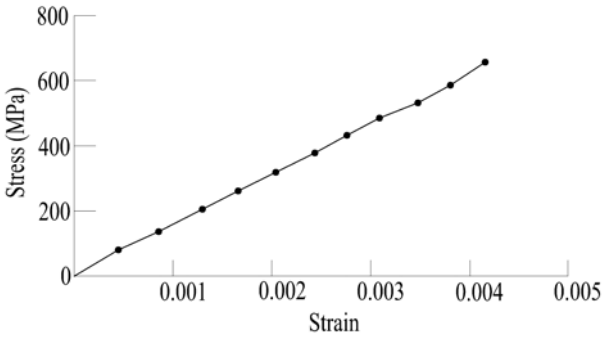

Figure 6. The stress-strain curve of the micro sample

4. Simulation, theory and experiment

In this paper, the threshold-value judging mechanism is taken as the research object. Based on the theory analysis, simulation analysis and experimental analysis, the response characteristics and the fracture mechanisms of the threshold-value judging mechanism are studied under the overload. In order to improve the design efficiency and shorten the research period, the threshold-value judging mechanism is simplified reasonably, according to the actual situation. The simplified threshold-value judging mechanism is fabricated, its main components are the centrifugal slider, threshold-value connection units and frame, as shown in Figure 7. The role of the threshold-value judging mechanism is as follows. In the usual state of service processing, when the ammunition accidentally falls or rolls ,the centrifugal slider can be kept in the original position because of the constraint of the threshold-value connection units in the threshold judging mechanism. Thereby, it can ensure the safety of the MEMS S&A device when the inertial safety device arming unexpected. In the process of launching, the centrifugal slider of the threshold-value connection units leads to the fracture failure under the centrifugal force, and the centrifugal slider starts to move, thereupon, it can ensure the reliability of the MEMS S&A device.

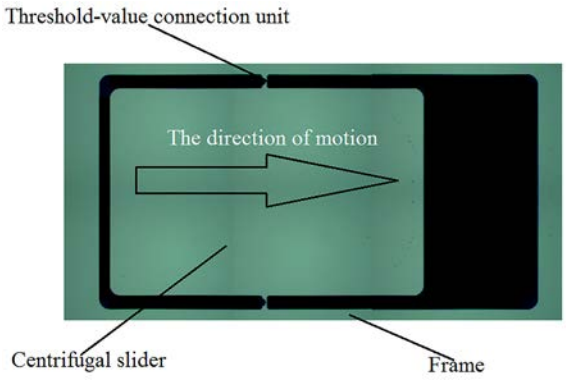

Figure 7. The fabricated threshold-value judging mechanism

4.1. Theory analysis

The threshold-value judging mechanism is a symmetric structure as shown in Figure 8. When the threshold-value judging mechanism is subjected to centrifugal acceleration overload, we can carry out the force analysis on one side of the structure.

Assuming that the centrifugal acceleration overload is a, then the centrifugal force of the centrifugal slider suffered is

$$F = ma . \quad (1)$$

The weak link of the threshold-value judging mechanism is the threshold-value connection units. Therefore, the complex stress problem of the threshold-value judging mechanism can be

Preprints (www.preprints.org) | NOT PEER-REVIEWED | Posted: 24 March 2017 doi:10.20944/preprints201703.0185.v1

simplified to the stress problem of the threshold-value connection units. Thereinto, the force of a threshold-value connection unit suffered is

$$F^{/} = \frac{F}{2} = \frac{ma}{2}. \tag{2}$$

Assuming that the size of the threshold-value connection units designed actually is shown in Figure 8, the minimum cross section of the threshold-value connection unit is actually a uniform beam because of the limitation of fabrication process. The stress analysis of the threshold-value connection unit is shown in Figure 8.

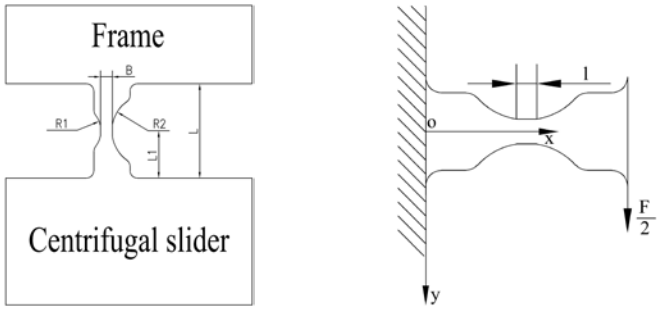

(**a**) (**b**)

Figure 8. (**a**) The parameters of the threshold-value connection unit; (**b**) The parameters and the stress analysis of the threshold-value connection unit.

Wherein, the span of the beam is L, $L1$ is the distance between the center of the circle arc and the root of the beam, the width of the minimum section of the beam is B, the thickness of the model is H, and the length of the uniform beam at the minimum section affected by the two circle arc radius $R1$ and $R2$ is l.

It is a plane stress problem of a cantilever beam with variable cross section, according to the Figure 9. Ignoring the volume force, and assuming that the width of the beam at different sections is $B(x)$, thus the differential equation of the stress component of the threshold-value connection unit is as follows.

$$\begin{cases} \dfrac{\partial \sigma_x}{\partial x} + \dfrac{\partial \tau_{xy}}{\partial y} = 0 \\ \dfrac{\partial \sigma_y}{\partial y} + \dfrac{\partial \tau_{xy}}{\partial x} = 0 \\ \left(\dfrac{\partial^2}{\partial x^2} + \dfrac{\partial^2}{\partial y^2} \right)(\sigma_x + \sigma_y) = 0 \end{cases}. \tag{3}$$

The boundary conditions are as follows.

$$\begin{cases} x = 0 : u = 0, v = 0 \\ x = l : \sigma_x = 0, \int_{-\frac{B(x)}{2}}^{\frac{B(x)}{2}} \tau_{xy} dy = \dfrac{F}{2} \\ y = \pm \dfrac{1}{2} B(x) : \sigma_y = 0, \tau_{xy} = 0 \end{cases}. \tag{4}$$

We can get the Eq.5 by the Eq.3 and theEq.4.

Preprints (www.preprints.org) | NOT PEER-REVIEWED | Posted: 24 March 2017 doi:10.20944/preprints201703.0185.v1

$$\begin{cases} \sigma_x = -\dfrac{F(L-x)}{2I_z} y \\ \sigma_y = 0 \\ \tau_{xy} = \dfrac{F}{4I_z}\left(\dfrac{B^2(x)}{4} - y^2\right) \end{cases} . \tag{5}$$

Wherein I_z is the moment of inertia of the threshold-value connection unit. Because the cross section is rectangular, we can get the formula as follows.

$$I_z = \frac{HB^3(x)}{12} . \tag{6}$$

By designing, the threshold-value judging mechanism is a symmetric structure and the centrifugal slider suffers almost all of the force. Moreover, the span of the centrifugal slider is much larger than the span of the threshold-value connection unit, therefore, the shear stress of the beam with variable cross section plays a leading role.

$$\tau_{xy} = \frac{F}{4I_z}\left(\frac{B^2(x)}{4} - y^2\right). \tag{7}$$

We can get the Eq.8 by takingEq.6 into Eq.7.

$$\tau_{xy} = \frac{3F}{4B^3(x)}\left(\frac{B^2(x)}{4} - y^2\right). \tag{8}$$

If we want to explore the weak point of the variable cross-section beam, it needs to get the maximum value of τ_{xy}. Because x and y are the independent unknowns, when $y = 0$, we can take the maximum value of τ_{xy}.

$$\tau_{xy} = \frac{3F}{4HB(x)}. \tag{9}$$

Therefore, we can take the maximum value of τ_{xy} as long as the $B(x)$ takes the minimum value for this variable cross-section beam.

Therefore, the maximum shear stress is as follows.

$$\tau_{xy} = \frac{3ma}{4HB} . \tag{10}$$

Furthermore, the minimum cross section of the threshold-value connection unit is actually a uniform beam with width of B and length of l because of the limitation of fabrication process. According to the knowledge of mechanics of materials, the bending stress of the threshold-value connection unit is mainly suffered by the uniform beam. In addition, the width of the uniform beam is much less than the width of the other beam in the threshold-value connection unit, so the force analysis of the uniform beam can be simplified to the force analysis of the cantilever beam, as shown in Figure 9.

Preprints (www.preprints.org) | NOT PEER-REVIEWED | Posted: 24 March 2017 doi:10.20944/preprints201703.0185.v1

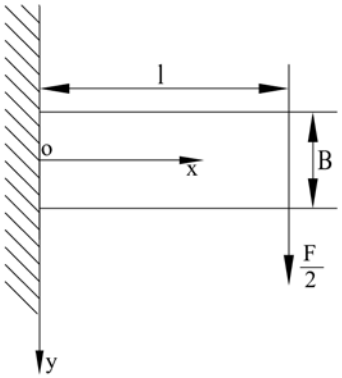

Figure 9. Mechanics analysis of the uniform beam.

The stress analysis of the cantilever beam is almost the same as that of the variable cross-section beam, we won't explore it here. The expression of the bending stress of the uniform beam is as follows.

$$\sigma_x = \frac{3mal}{HB^2}. \tag{11}$$

As is stated above, the average fracture strength of the silicon material is $\sigma_s = 726\text{MPa}$. Thus, we can obtain the expression of the maximum resultant stress for the minimum cross section by combining τ_{xy} and σ_x, and the expression of the resultant stress is shown in Eq.12.

$$\sigma_s = \sqrt{\sigma_x^2 + \tau_{xy}^2} = 726\text{MPa}. \tag{12}$$

According to the design, $L = 0.13mm = 1.3\times10^{-4}m$ $B = 0.015mm = 1.5\times10^{-5}m$, $H = 0.4mm = 4\times10^{-4}m$, $l = 0.013mm = 1.3\times10^{-5}m$, the centrifugal slider mass $m = 5.2\times10^{-6}Kg$. Thus, we can get the below result.

$$a = 2.9162\times10^5 m/s^2. \tag{13}$$

Therefore, when the threshold-value judging mechanism is subjected to the acceleration overload of 29162g, the weak links of the threshold-value connection units occur fracture failure.

In addition, the distance between the barycenter of the sub-centrifugal slider and the rotation axis of the projectile is $r = 6mm$, as can be seen in Figure 2. When the rotation angular velocity of the projectile is ω, the centrifugal acceleration of the centrifugal slider a_0 can be calculated by the following formula.

$$a_0 = r\omega^2. \tag{13}$$

It is known that the maximum rotating speed of the projectile is 73918r/min, then from above formula we can obtain that the maximum centrifugal acceleration of the centrifugal slider is $a_0^{max} = 359508m/s^2$.

Through above analysis and discussion, we can get the result of $a_0^{max} > a$, so in theory, the threshold-value judging mechanism which our term designed can realize reliable arming under the centrifugal overload of the 35mm caliber launching ammunition.

4.1. Experimental and simulation analysis

The experiment schemes are mainly to achieve the dynamic response characteristics of the threshold-value judging mechanism under the drop overload of service processing and the centrifugal overload of the launching ammunition, as shown in Table 2.

 doi:10.20944/preprints201703.0185.v1

Table 2. The experiment schemes and the verification contents.

Experiment schemes	Verification contents
Hopkinson impact experiment	Fracture performance of the threshold-value judging mechanism under the drop overload
High speed centrifugal experiment	Fracture performance of the threshold-value judging mechanism under the centrifugal overload

According to the characteristics of small size and light weight of the MEMS S&A device, our term has designed and built a set of magnetic resistance Hopkinson impact system which has the advantage of adjustable threshold-value, good repeatability and high precision (see Figure 10). The system generates the overload by using the electromagnetic emission device which launches bullet to impact the compressed bar, the impact overload can be up to 45000g, and the experiment frequency is several minutes each time. In addition, in order to meet the requirements of fast experiment of MEMS S&A device, we designed the installation and fixing mechanism of the micro sample according to the content of this experiment, as shown in Figure 11.

The working principle of the magnetic resistance Hopkinson impact system is as follows. According to the required overload value, the corresponding charge is added to the electrolytic capacitor, and then connect the electrolytic capacitor to the electromagnetic coil. When the control circuit is identified as a working state, the electrolytic capacitor is instantly discharged to generate a strong current flowing through the electromagnetic coil. A strong magnetic field which is parallel to the coil is generated in the electromagnetic coil, at the same time，the bullet in the electromagnetic emission device is magnetized and then the bullet is ejected. When the bullet is flying out of the electromagnetic emission device, the bullet drives the photoelectric switch to disconnect electromagnetic coil, and finally the bullet impacts the compressed bar which is equipped with micro sample and acceleration sensor.

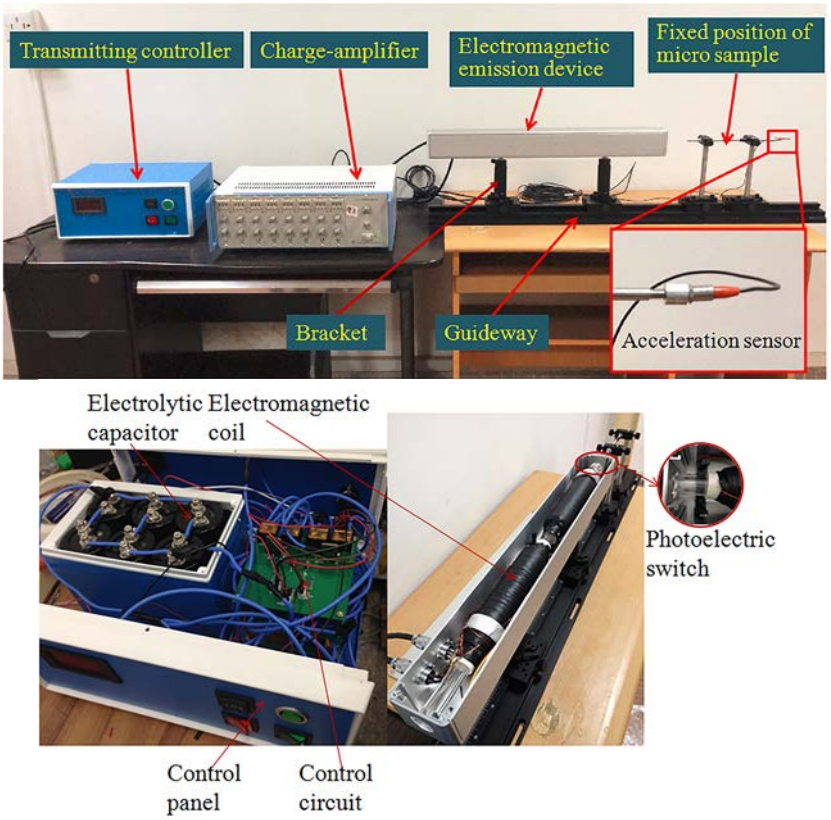

Figure 10. The composition of the magnetic resistance Hopkinson impact system.

Preprints (www.preprints.org) | NOT PEER-REVIEWED | Posted: 24 March 2017 doi:10.20944/preprints201703.0185.v1

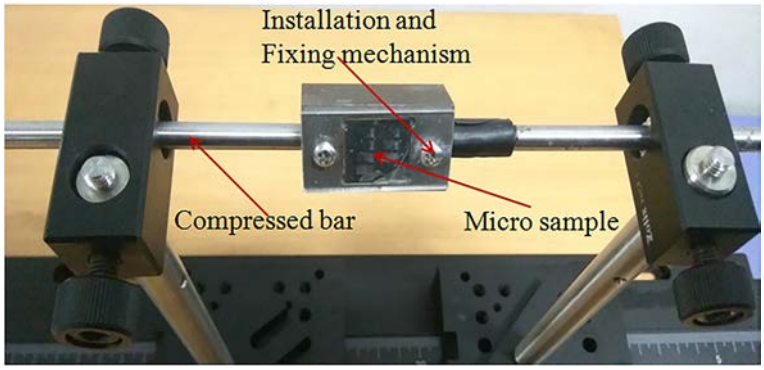

Figure 11. The installation and fixing mechanism of the micro sample.

As can be seen from Figure 2, the overload peak is 12000g for the drop overload. The impact experiment is carried out on the threshold-value judging mechanism by using the magnetic resistance Hopkinson impact system as shown in Figure 11. In addition, in order to demonstrate whether the design safety margin of the threshold-value judging mechanism is sufficient, the overload peak set between 12000g and 21000g. The motion direction of centrifugal slider under the impact acceleration is shown in Figure 7, and the experiment results are shown in table 3.

Table 3. The Hopkinson impact experiment results.

Number	Charging voltage (V)	Acceleration Peak value (g)	Pulse width (μs)	Fracture situation
1	72 (Single-stage)	14113	50	NO
2	82 (Single-stage)	16155	50	NO
3	91 (Single-stage)	18231	50	NO
4	99 (Single-stage)	20526	50	NO

From the above table, we can see that the threshold-value judging mechanism cannot occur fracture failure when the acceleration peak value is 20526g. Because of the overload peak is 12000g for the drop overload, the designed threshold-value judging mechanism can meet the design requirements of MEMS S&A device and has sufficient design safety margin.

In the case of the threshold-value judging mechanism under the centrifugal overload of the launching ammunition, centrifugal experiments are carried out by using a centrifugal tooling as shown in Fig 12. The maximum rotating speed of the centrifuge is 20000r/min, and the eccentricity of the micro sample is 100. Thus, the maximum centrifugal overload of micro sample is up to 43865g. We carried out the parameter design of the threshold-value connection units, and the fabricated threshold-value judging mechanism as shown in Figure 13. We take the centrifugal acceleration of 10000g as the initial value and 1000g as step length, and explored the fatigue limit for fracture of the threshold-value connection units as shown in Table 4.

Figure 12. Centrifugal experiment platform and centrifugal tooling.

Preprints (www.preprints.org) | NOT PEER-REVIEWED | Posted: 24 March 2017 doi:10.20944/preprints201703.0185.v1

The finite element models (see Figure 13) are established by using HyperMesh for the parameterized threshold-value connection units as shown in Table 4. At the same time, according to the theoretical analysis results, we take the centrifugal acceleration of 29000g as the initial value and 100g as step length, explore the fatigue limit for fracture of the threshold-value connection units as shown in Table 4.

Through theoretical analysis, simulation analysis and experimental study, we can get the results as shown in Table 4 and Figure 14.

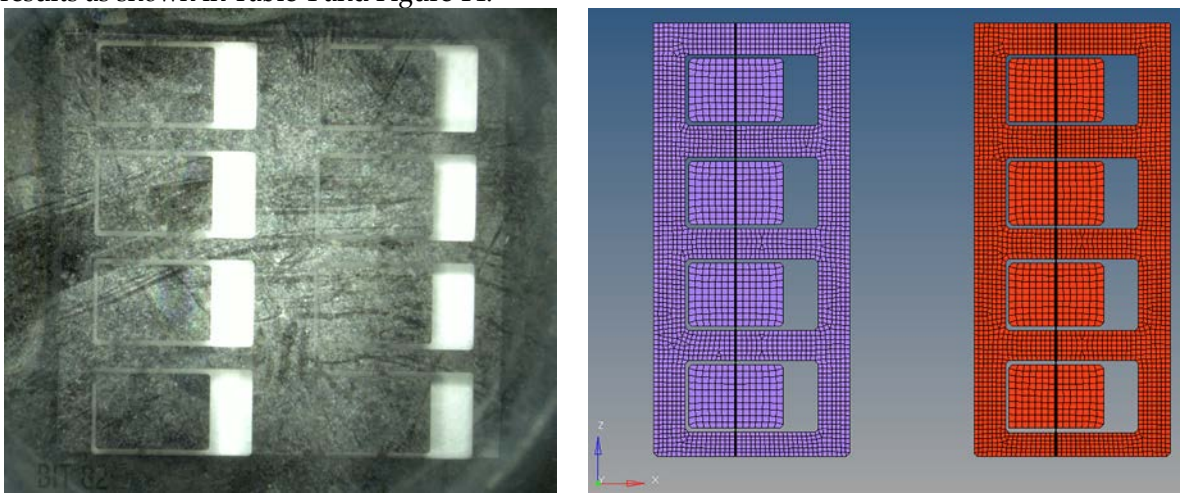

(**a**) (**b**)

Figure 13. (**a**) Principle prototypes of threshold-value judging mechanism; (**b**) Finite element models of threshold-value judging mechanism.

Table 4. The key parameter values of different threshold-value connection units and the corresponding g values of arming for the threshold-value judging mechanism

Number	The key parameter value (μm)				The g value of arming for the threshold-value judging mechanism					
					Experimental results				Theoretical results	Simulation results
	R1	R2	B	L1	Group 1	Group 2	Group 3	Average		
a)	42.5	42.5	15	65	32000g	30000g	34000g	32000g	29162g	28200g
b1)	40	42.5	15	65	31000g	35000g	33000g	33000g	30833g	29100g
b2)	35	42.5	15	65	35000g	39000g	37000g	37000g	34800g	33000g
b3)	45	42.5	15	65	30000g	31000g	35000g	32000g	29162g	28100g
b4)	50	42.5	15	65	31000g	30000g	32000g	31000g	29162g	28000g
c1)	42.5	40	15	65	34000g	32000g	31000g	32333g	30833g	29100g
c2)	42.5	35	15	65	38000g	34000g	36000g	36000g	34800g	33000g
c3)	42.5	45	15	65	29000g	33000g	31000g	31000g	29162g	28100g
c4)	42.5	50	15	65	30000g	28000g	35000g	31000g	29162g	28000g
d1)	42.5	42.5	13	65	27000g	23000g	25000g	25000g	22116g	21100g
d2)	42.5	42.5	12	65	20000g	21000g	22000g	21000g	18927g	18000g
d3)	42.5	42.5	16	65	37000g	35000g	36000g	36000g	33005g	31600g
d4)	42.5	42.5	17	65	38000g	41000g	42000g	40333g	37054g	35400g
e1)	42.5	42.5	15	60	34000g	33000g	32000g	33000g	29162g	28300g
e2)	42.5	42.5	15	55	33000g	33000g	34000g	33333g	29162g	28500g
e3)	42.5	42.5	15	70	31000g	30000g	32000g	31000g	29162g	28000g
e4)	42.5	42.5	15	75	30000g	31000g	30000g	30333g	29162g	27800g

Preprints (www.preprints.org) | NOT PEER-REVIEWED | Posted: 24 March 2017 doi:10.20944/preprints201703.0185.v1

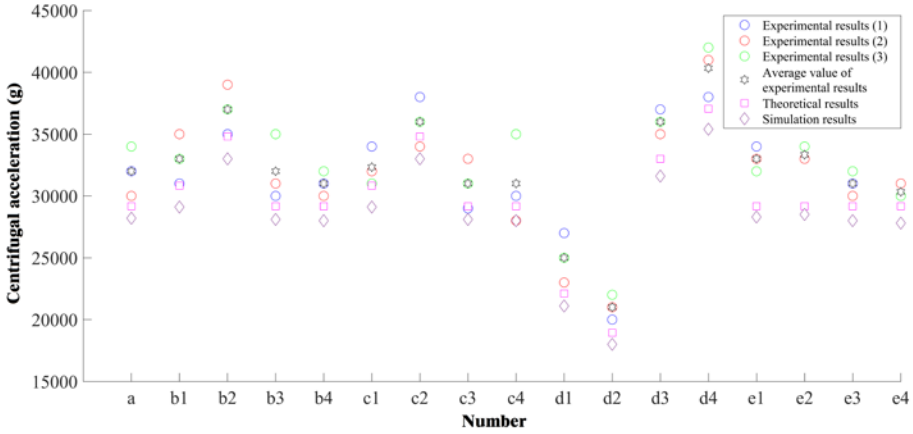

Figure 14. The g values of arming forparameterized threshold-value judging mechanism.

According to Table 4 and Figure 14, the conclusions we obtained is as follows.

(1) Through the results of theory, simulation and experiment, we can know that the fracture threshold-value of the threshold-value judging mechanism is 29162g, 28200g and 32000g, respectively, all of which are much less than 35951g of the design principle. The threshold-value judging mechanism meets design requirements of MEMS S&A device.

(2) In the same fabrication batch and same design parameters of the threshold-value judging mechanism, there is a larger discreteness in the g values of arming. this conclusion illustrates that the certain discreteness exists in the mechanical properties of silicon material. Therefore, the certain discreteness should be taken into account at the design process.

(3) The study shows the theoretical results are higher than the simulation results. The reason is the effect on the structural strength from the structure parameters, such as L1, is ignored and the theoretical calculation is static method.

(4) The average experimental results in the study are higher than the theoretical results. This situation is caused by the friction and gas damping existed in micro samples.

(5) The theoretical results, the simulation results and the experimental results have a high consistency. The conclusion illustrate we can carry out initial optimization design through the theoretical method.

5. Conclusions

According to a MEMS S&A device designed by our term, this paper introduces its design principle and fabrication process. At the same time, we also illustrate the design requirements of modules in MEMS S&A device. Taking the threshold-value judging mechanism as the study object, this paper aims to verify the feasibility of the designed threshold-value judging mechanism in MEMS S&A device. The simplified threshold-value judging mechanism is fabricated and the mechanical properties of silicon materials are tested. From the tensile tests, we obtain that the average fracture strength and Young's modulus of silicon are 726Mpa and 175GPa, respectively.Through using the theoretical method, simulation method and experimental method to study the the fracture mechanism of the threshold-value judging mechanism under the drop overload of service processing and the centrifugal overload of the launching ammunition. From Hopkinson impact experiment, we can get that the threshold-value judging mechanism is safety under the impact overload of 20526g, this value is much more than the standard of the drop overload 12000g; the arming value under the centrifugal overload obtained from theory, simulation and experiment is at the range of 28200g and 32000g, it shows that the threshold-value judging mechanism can be arming compared with the value 35951g of design principle. Therefore, it can confirm the threshold-value judging mechanism meets design requirements. The relationship of fracture threshold-values obtained by different methods is found out through parametric design

method, as shown in Figure 14, the research can provide fundamental knowledge for optimizing model parameters.

Acknowledgments: The research is supported by the State Key Laboratory of Mechatronics Engineering and Control and sponsored by National Project (No. Z092014B001 and No. B3320132011).

Author Contributions: W.-Z.L. conceived the problem and designed the solution; F.-F.W. and Y.F. designed the experiments; C.-S.C. performed the experiments; F.-F.W. and D.-K.W. analyzed the data; D.-K.W. wrote the paper.

Conflicts of Interest: The authors declare no conflict of interest.

References

1. Onkar, K.; Sujay, G.; Ankush, H. Safety and Arming Mechanism (SAM) for Mortar Fuze.International Journal for Scientific Research & Development. 2015, 3,637-639.
2. Fan, G.x.; Li, J.H. Design and Analysis of MEMS Linear Phased Array. Micromachines. 2016, 7, 8; doi:10.3390/mi7010008.
3. Shaeffer, D.K. MEMS inertial sensors: a tutorial overview. IEEE Commun. Mag. 2013, 51, 100-109.
4. Han, K.; Deng, Z.L.; Guo, X.B. Design and Analysis of a Silicon-Based Pattern Reconfigurable Antenna Employing an Active Element Pattern Method. Micromachines. 2017, 8, 11; doi:10.3390/mi8010011.
5. Wang, Y.; Lou, W.Z.; Feng, Y. High impact dynamic simulation of planar S-form micro-spring. Key Eng. Mater. 2013, 562, 1107-1110.
6. Jeong, B.W.; Kim, M.O. Development of MEMS Multi-Mode Electrostatic Energy Harvester Based on the SOI Process. Micromachines. 2017, 8, 51; doi:10.3390/mi8020051.
7. Ozdogan, M.; Towfighian, S. Nonlinear Dynamic Behavior of a Bi-Axial Torsional MEMS Mirror with Sidewall Electrodes. Micromachines. 2016, 7, 42; doi:10.3390/mi7030042.
8. Deng, Z.L.; Guo, X.B. Design, Analysis, and Verification of Ka-Band Pattern Reconfigurable Patch Antenna Using RF MEMS Switches. Micromachines. 2016, 7, 144; doi:10.3390/mi7080144.
9. Jiang, X.H.; Yin, Q.; Tian, Y. Study on MEMS initiators. Initiat Pyrotech. 2009, 6, 11-13.
10. Pezous, H.; Rossi, C.; Sanchez, M. Fabrication, assembly and tests of a MEMS-based safe, arm and fire device. Journal of Physics and Chemistry of Solids. 2010, 71, 75-79.
11. Wang, S.W.; Hao, Y.P.; Zhang, D.Z. The comprehensive analysis of MEMS-based fuze safety and arming device. Detect Control. 2006, 28, 55-58.
12. Hélène, P.; Carole, R.; Marjorie, S. Integration of MEMS based safe arm and fire device. Sensors & Actuators A Physical. 2010, 159,157-167.
13. Feng, P.Z.; Zhu, J.N.; Wu, Z.L. Analysis of US typical MEMS fuze safety & arming device. Detect Control. 2007, 29, 26-30.
14. Pezous, H.; Rossi, C. ; Sanchez, M. Fabrication, assembly and tests of a MEMS-based safe, arm and fire device. Phys Chem Solids. 2010, 71, 75-79.
15. Robinson, C.H. Ultra-miniature, monolithic, mechanical safety-and- arming (S&A) device for projected munitions. USP: 6064013, 2001.
16. Li, X.; Zhao, Y.; Hu, T. Design of a large displacement thermal actuator with a cascaded V-beam amplification for MEMS safety-and-arming devices. Microsystem Technologies. 2015, 21, 2367-2374.
17. Bao, B.; Yan, N.; Geng, W. Simulation and experiment investigation on structural design and reinforcement of pyrotechnical sliding micro-actuators. Analog Integrated Circuits and Signal Processing, 2016, 88, 1-11.
18. Cochran, K.R.; Fan, L.; DeVoe, C.L. Moving reflector type micro optical switch for high-power transfer in a MEMS-based safety and arming system. Journal of Micromechanics and Microengineering. 2003, 14, 138-146.
19. He, G. Micro-mechanical safety mechanism based on MEMS technology theory and application. Thesis, Beijing Institute of technology, Beijing, 2006.
20. Zhou, Z.J.; Nie, W.R.; Wan, X.F. Study on Parameters of MEMS Planar Zigzag Slot for Fuze. Key Engineering Materials. 2014, 609, 813-818.
21. Feng, Y.; Hagiwara, K.; Iguchi, Y. Trench-filled Cellular Parylene Electret for Piezoelectric Transducer. Appl. Phys. Lett. 2012,100, 262901-262901.4.

22. Peng, S.W.; Shih, P.J.; Dai, C.L. Manufacturing and Characterization of a Thermoelectric Energy Harvester Using the CMOS-MEMS Technology. Micromachines. 2015, 6, 1560–1568; doi:10.3390/mi6101439.
23. Lin, C.Y.; Hsu, C.C.; Dai, C.L. Fabrication of a Micromachined Capacitive Switch Using the CMOS-MEMS Technology. Micromachines. 2015, 6, 1645–1654; doi:10.3390/mi6111447.
24. Ozdemir, S.; Akhtar. S. Measuring the Quality Factor in MEMS Devices. Micromachines. 2015, 6, 1935–1945; doi:10.3390/mi6121466.
25. Zhao, Y.L.; Hu, T.J.; Li, X.Y. Design and Characterization of a Large Displacement Electro-Thermal Actuator for a New Kind of Safety-and-Arming Device. Energy Harvesting & Systems. 2015, 2, 143-148.
26. Jiang, B.; Qi, X.L.; Zhao, Z.N. Key Technologies Research of MEMS Pressure Sensor for Fuze. J. Applied Mechanics and Materials. 2014, 472,242-246.
27. One, k.R.; Sung, S.K.; Jae, W.B. Simplified Parametric Study on M125 Booster Mechanism and its Application for Determining the Characteristic Constant of Arming Distance. Journal of the KIMST. 2015, 18,409-414.
28. Bao, B.; Yan, N.; Geng, W. Simulation and experiment investigation on structural design and reinforcement of pyrotechnical sliding micro-actuators. Analog Integrated Circuits and Signal Processing. 2016, 88(3):1-11.
29. Liu, J.K.; Qi X.L.; Jia, J. Study on the Reliability Problem of MEMS Fuze Mechanism. Advanced Materials Research. 2012, 628, 72-77.
30. Jakob, G.; Per, D.; Helge, K. Use of conductive adhesive for MEMS interconnection in ammunition fuze applications. Journal of Micro/Nanolithography, MEMS, and MOEMS. 2010, 9, 1-10.
31. XIE, R.Z.; Ren, X.M. Research on design and firing performance of Si-based detonator. Defence Technology. 2014, 10, 34-39.
32. Wang, F.F.; Lou W.Z. The Parametric Analysis of the Lock-Releasing Mechanism in MEMS Safety and Arming Device. Key Engineering Materials. 2015,645, 986-989.
33. Wang, F.F.; Lou, W.Z.; Feng, Y. Fracture Mechanism of Movable Part in Micro-electro-mechanical Systems Device Based on Empirical Electron Theory. Micro & Nano Letters. 2016, 11, 29-33.
34. Wang, F.F.; Lou, W.Z.; Wang, Y. Design and Analysis of a Novel Locking Mechanism of MEMS Safety and Arming Device. Key Engineering Materials. 2014,609, 856-859.